HT2023-106939

REMOTE THERMAL MEASUREMENTS WITH REGRESSION OF ACOUSTIC EMISSIONS

Christy Dunlap
University of Arkansas,
Department of
Mechanical
Engineering
Fayetteville, AR

Hari Pandey
University of Arkansas,
Department of
Mechanical
Engineering
Fayetteville, AR

Jackson Marsh
University of Arkansas,
Department of
Mechanical
Engineering
Fayetteville, AR

Ethan Weems
University of Arkansas,
Department of
Mechanical
Engineering
Fayetteville, AR

Han Hu

University of Arkansas, Department of Mechanical Engineering Fayetteville, AR

ABSTRACT

Real-time thermal monitoring and regulation are critical to the mitigation of thermal runaways and device failures in twophase cooling systems. Compared to conventional approaches that rely on the Joule effect, thermal gradient or transverse thermoelectric effect, acoustic emission (AE)-based remote sensing is more promising for robust and non-intrusive thermal monitoring. Nevertheless, due to the high stochasticity and noise of acoustic signals, existing implementations of AE in thermal systems have been limited to qualitative state monitoring. In this paper, we present a technology for real-time heat flux quantification during two-phase cooling by coupling acoustic sensing using hydrophones and condenser microphones and regression-based machine learning frameworks. frameworks integrate a fast Fourier transform feature extraction algorithm with regressors, i.e., Gaussian process regressor and multilayer perceptron regressor for heat flux predictions. The acoustic signals and heat fluxes are collected from pool boiling tests under transient heat loads. It is shown that both hydrophone and condenser microphone signals are successful in predicting heat flux. Multiple models are trained and compared some using only one form of acoustic data while others combine both acoustic types (i.e., hydrophone and microphone) in fusion ML models (i.e., early, joint, late). The models using only hydrophone data are shown to perform better than the models using only microphone data. Also, some forms of fusion are shown to have better performance than either of the single input data type models. This AE-ML technology is demonstrated for accurate heat flux quantification. As such, this work will not only lead to a light, low-cost, and non-contact thermal measurement technology but also a new perspective for the physical explanation of bubble dynamics during boiling.

Keywords: Pool Boiling, Heat Flux, Hydrophone, Microphone, Acoustics, Machine Learning, Gaussian Process Regression

1. INTRODUCTION

High-performance cooling schemes are needed to sustain the growth of high-power density applications, e.g., data centers [1] and electric vehicles [2]. Two-phase cooling has the potential to meet these cooling needs by providing greater heat flux dissipation while maintaining a relatively low wall superheat in the nucleate boiling regime. However, two-phase cooling is limited by instabilities such as critical heat flux (CHF) and a lack of understanding of boiling dynamics [3]. Due to this, in order to avoid overheating or burnout, fast and accurate monitoring of the cooling system is crucial for successful implementation.

Intrusive heat flux quantification methods have been used during pool boiling, e.g., the Joule effect method [4], gradient method [5], [6], or transverse thermoelectric effect [7]. For the Joule effect method, heat flux is calculated directly using the voltage and current applied. It is used for experiments where the ratio of boiling surface area to total surface area is large. For the gradient method, the temperature difference is measured within a material with known thermal conductivity (k) and then Fourier's law $(q = -k \nabla T)$ is used to calculate the heat flux. Although these methods are relatively easy and cheap to implement, they suffer from drawbacks. The joule effect method

is subject to large errors from nonuniform heating and the response time of the gradient method is limited by thermal diffusion. Also, since these methods require sensors embedded near the heating surface, they can be difficult to replace and can interfere with the boiling dynamics.

To avoid such interference, nonintrusive methods, such as optical or acoustic sensing methods, are desired. Image processing is one area that is been studied extensively in pool boiling [8]-[10]. Traditional image analysis has been used to correlate heat flux to boiling features within the image [11] (e.g., bubble diameter or bubble count). Advances in computer vision have also aided in faster and more accurate pool boiling image processing. Some groups have used image-based machine learning methods for predicting heat flux. Suh et al used features extracted using a convolutional neural network (i.e., VGG16) with physical bubble features such as count and size found from Mask R-CNN [12]. These features were then used in an MLP to predict heat flux. Hobold et al used the unsupervised principal component analysis (PCA) method to extract features which were then used in training and testing an mlp for heat flux prediction [13]. Although the data collection system utilizing a camera can be entirely nonintrusive, the setup presents challenges in an actual implementation such as the size/ weight of the system or the need for a transparent boiling chamber and adequate light.

Acoustic sensing is nonintrusive, low-cost, light, and easy to implement [14]. A variety of acoustic sensors have been implemented in boiling studies such as AE sensors, hydrophones, and condenser microphones. Hydrophones are submerged in the body of liquid so they can be placed close to the boiling surface. Condenser microphones are placed outside of the boiling set up allowing for a truly non-intrusive sensor, however, they are subject to high levels of noise. Current studies have drawn connections between raw signals, power spectral density, frequency domain, etc. to boiling characteristics. Alhashan et al. correlated data from acoustic emission sensors (e.g., AE energy, RMS, amplitude, etc.,) to fluid viscosity and bubble diameter [15]. Baek et al found that the AE hit number increased with heat flux [16]. Nishant et al observed a sharp increase in the intensity of the acoustic signals at the CHF during pool boiling experiments at different subcooling [17]. Machine learning has also been incorporated with acoustic signals for various applications like anomaly detection [18], guitar effects recognition [19], or monitoring gas-liquid mixing [20]. With respect to boiling studies, coupling machine learning techniques and acoustic sensing have been less explored. Its uses have been limited to qualitative analysis such as boiling regime classification. Sinha et al used acoustic signals from pool boiling to predict the associated boiling regime [21]. They did this by transforming the acoustic signal to a spectrogram then used CNN for feature extraction and an MLP classification model to predict the regime. Ueki and Ara used an MLP model for classifying boiling regimes using sound pressure levels from a hydrophone [22]. One drawback of acoustic sensing is that they suffer from high noise levels. Especially in boiling studies, it can be difficult to remove noise while maintaining important features from

boiling. Some groups just use the raw signal while others have performed some noise filtering. Negi used Audacity to filter the noise from their signal by using a portion of the signal where only the noise was present and boiling was not taking place [23].

In this work, both condenser microphone and hydrophone signals from a pool boiling experiment are used to train and test machine learning models for predicting heat flux. These quantitative models include multilayer perceptron and Gaussian process regression models. Both data types are used independently and together in different types of simple fusion models.

2. MATERIALS AND METHODS

Data from a pool boiling experiment was collected and preprocessed. This section describes the experimental setup for collecting the data, how the data was processed for use in the machine learning models, and the structure of the supervised regression machine learning models.

2.1 Data Collection

Data were collected from a transient pool boiling experiment where the heat load ramps up to initiate the critical heat flux condition. A 1cm × 1cm copper block with surface structures is summurged in deionized water heated to its saturation point. The block is heated with nine cartridge heaters (Omega Engineering IIDC19102) connected to a DC power supply (Magna-Power SL200-7.5) past the CHF. Four Type-T thermocouples (Omega Engineering TJ36-CPSS-032U-6) are evenly spaced in the copper block with a spacing of 0.1 inches and are connected to an NI DAQ module (NI 9210). The thermocouples were set to a sampling rate of 3012 Hz. More detailed facility description and test procedures are provided in [24] and [25], [26], respectively. **Figure 1** shows the recorded temperatures in the copper block with the four thermocouples and the heat flux calculated using Fourier's law.

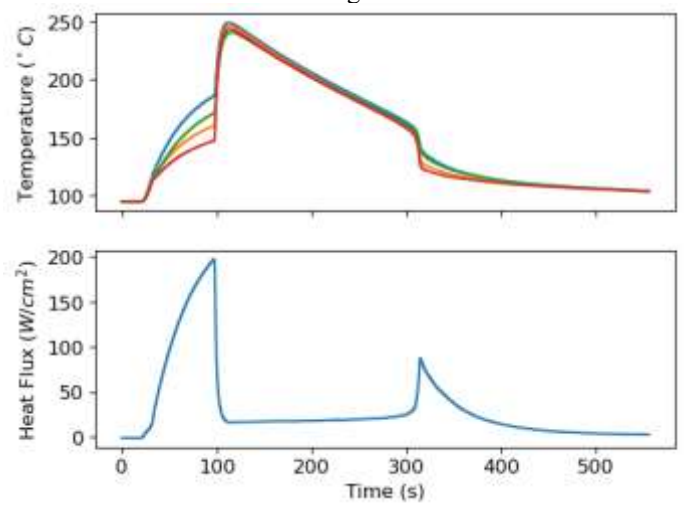


FIGURE 1 : TEMPERATURE FROM THERMOCOUPLES AND CALCULATED HEAT FLUX AS A FUNCTION OF TIME.

For the acoustic data sampling, both a hydrophone and condenser microphone were used. A hydrophone with a built-in preamplifier (High Tech HTI-96-Min) was submerged near the

copper surface in the boiling chamber. A condenser microphone (Behringer ECM8000) was used to measure AE outside of the boiling chamber. The microphone was placed directly outside of the chamber and was pointed at the nucleation source, to ensure the best results despite its omnidirectional capability. The microphone reads from 15Hz-20kHz. A 48V phantom power supply (Neewer NW-100) was used to power the microphone. This was then connected to the main DAQ body (Behringer U-PHORIA UMC404HD). The DAQ can relay signals of 10Hz-43kHz. This interface also allows for the preamplification of the signal. The DAQ was connected to the computer and the data was collected via LabVIEW. Both the hydrophone and microphone were set to a sampling rate of 3012 Hz. Noise removal is a difficult task for pool boiling acoustics in the sense that it is easy to remove important characteristic acoustic boiling features within the signal. Audacity was used to attempt to remove some of the noise from the microphone signal. To do this, the noise reduction effect in Audacity was used. The microphone signal was first scaled to have an absolute max of 1 and saved as a wav file for use in Audacity. A sample of the signal near the end was used as the noise profile and the settings 12 dB, 5 sensitivity, and 1 frequency smoothing were selected. This noise filtering was applied to the entirety of the microphone signal. Figure 2 shows the hydrophone acoustic signals and both the raw microphone signal and the filtered microphone signal. Both the raw microphone signal and noise-reduced signal were used in the machine learning models.

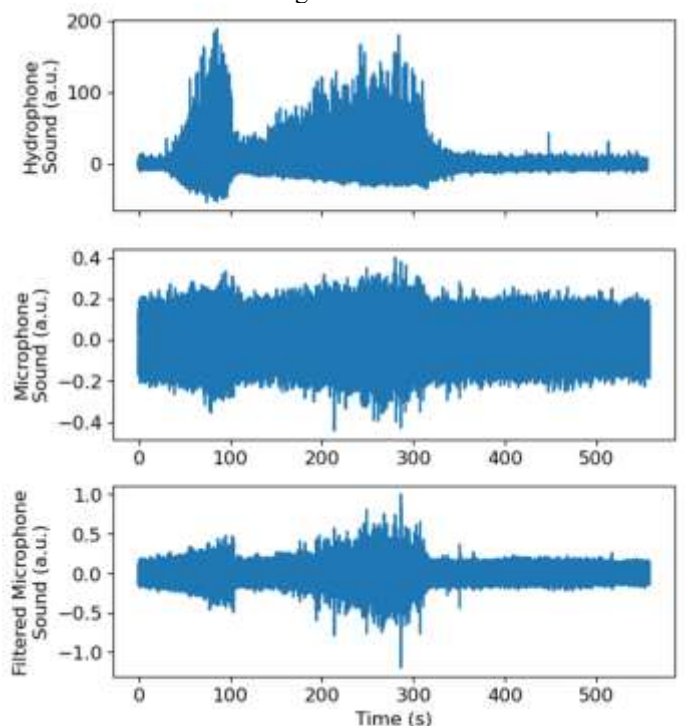


FIGURE 2: ORIGINAL HYDROPHONE AND MICROPHONE DATA AND FILTERED MICROPHONE DATA.

2.2 Data Preparation

Figure 3 shows an overview of the process used in for the models. The sound data collected from the experiment was segmented and then converted to sets of frequency intensity vectors which were then used in different types of regression models. This was done for both the raw signals and the filtered microphone data. This section describes the methods used for processing the data including the signal segmentation and feature extraction.

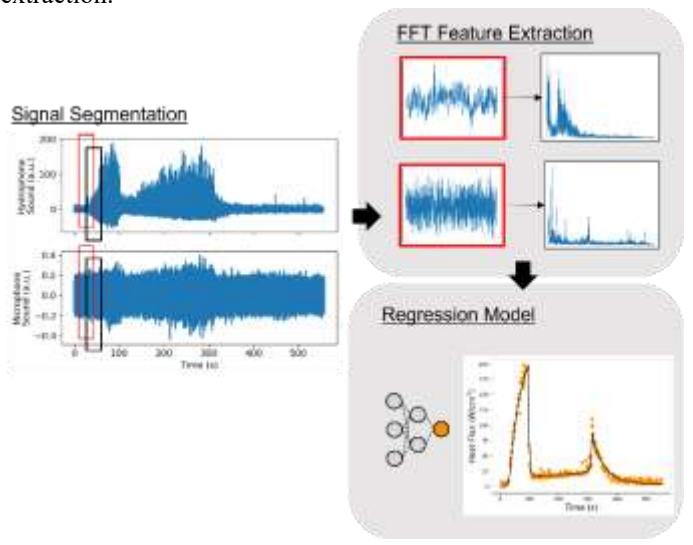


FIGURE 3: SCHEMATIC OF THE GENERAL PROCESS OF CONSTRUCTING THE MODELS.

Five supervised mlp sequential regression models and three Gaussian process regression models were used to predict heat flux. The microphone, hydrophone, and thermocouples were sampled at the same rate (3012 Hz). However, they all had different data collection start times and lengths. To account for this the beginning and end of the microphone and hydrophone signals were cropped to match the thermocouples' start and end time. After cropping, the dataset consisted of three equal-length sequences of data; hydrophone (S_H), microphone (S_M), and heat flux (H).

$$S_{H} = \{s_{h}(t_{0}), s_{h}(t_{1}), \dots s_{h}(t_{N-1})\}$$

$$S_{M} = \{s_{m}(t_{0}), s_{m}(t_{1}), \dots, s_{m}(t_{N-1})\}$$

$$H = \{h(t_{0}), h(t_{1}), \dots, h(t_{N-1})\}$$

where $s_H(t_i)$ is a hydrophone sample at time t_i , $s_M(t_i)$ is a microphone sample at time t_i , $h(t_i)$ is a calculated approximation of heat flux at time t_i , and N is the number of samples in the sequences.

The machine learning models take in inputs of audio sequences and output a single heat flux prediction value. The audio data needed to be split into sequences and matched to a heat flux. To create these sequences, a rolling sampling method was used for the acoustic signals with some overlap to create a larger data set. Both the hydrophone and microphone sequences (S_H, S_M) were split into sets of shorter audio clips;

split into sets of shorter audio clip
$$\{a_h^0, a_h^1, \dots a_h^{((N-1)-N_{seq})/N_{stride}}\}\$$
 $\{a_m^0, a_m^1, \dots, a_m^{((N-1)-N_{seq})/N_{stride}}\}\$

where each a_h^i and a_m^i are shorter audio clips of the hydrophone and microphone data respectively and defined as:

 $a_h^i = \{s_h(t_{i*N_{stride}}), s_h(t_{i*N_{stride}+1}), \dots, s_h(t_{i*N_{stride}+N_{seq}})\},$ $a_m^i = \{s_m(t_{i*N_{stride}}), s_m(t_{i*N_{stride}+1}), \dots, s_m(t_{i*N_{stride}+N_{seq}})\},$ $N_{seq} \text{ is the sequence length (i.e. length of the sequence segments } (a_h^i, a_m^i)) \text{ and } N_{stride} \text{ is the stride (i.e. amount of samples to skip before the starting term in the next sequence segment). Each audio sequence segment was then matched to a calculated heat flux which corresponds to the same time as the last audio sample in the sequence. Or in other words, each <math>a_h^i, a_m^i$ is matched to the heat flux value $h(t_{i*N_{stride}+N_{seq}}).$

The dataset used for all the models was prepared with a sequence length of 4000 and a stride of 1000. Next each sequence segment (a_h^i, a_m^i) was converted to frequency features using the fast Fourier transform (FFT). This was done using the FFT function in the NumPy library [27].

2.3 Machine Learning Models

Two different machine learning regression model architectures were used; multilayer perceptron (mlp) and Gaussian process regression. For each model architecture type, two of the models were trained using only hydrophone or only microphone data and the remaining models used a combination of both types of data in fusion models. For all the models, 80% of the data was used for training while 20% was used for testing. For the mlp models, 20% of the training data was used for validation. All of the models used the same training data and testing data.

Four different mlp model architectures were trained and tested on the hydrophone and microphone data seperately. The architecture which had the best performance on the test data for both the hydrophone and microphone data was chosen for further analysis and for use in the feature extraction portion of the fusion models. An mlp is a machine learning model that consists of layers of neurons. Each neuron describes a function whose inputs are first each multiplied by a weight then summed with a bias and passed through an activation function. A common activation function is the rectified linear unit (ReLU) which is defined as $f(x) = \max(0, x)$. During training, backpropagation is used to iteratively update the weights and biases to minimize the specified loss. In supervised learning, the loss function is defined to describe the difference between the model's prediction and true label. For example, the mean squared error loss function is commonly used in regression problems and defined as MSE = $\frac{1}{N} \sum_{i=1}^{N} (true_i - pred_i)^2$. The hydrophone data only and microphone data only models had an identical structure shown in Figure 4. The models consisted of 6 dense layers with 200, 200, 200, 200, 64, and 1 neurons respectively. The first 5 layers used the ReLU activation function. Dropout after the 2nd, 4th, and 6th layer was implemented with a rate of 0.2. Dropout is used to prevent overfitting during training by randomly dropping inputs at a specified rate for the layer.

Three types of fusion were implemented on the data; early, joint, and late. Figure 5 shows the general structure of the

three types of fusion used. The fusion models all took in inputs of both hydrophone and microphone frequency features. The difference between the three models residing in the concatenating location. The early fusion model concatenated the hydrophone and microphone frequency features first then passed these frequencies through an mlp which consisted of 6 dense layers with 200, 200, 200, 200, 64, and 1 neurons. The first 5 layers used the ReLU activation function. Two dropout layers with a rate of 0.2 were applied after the 2nd and 4th layer. For the joint fusion model, the hydrophone and microphone frequency features were first passed through mlps separately. These mlps consisted of 2 dense layers with 200 and 200 neurons, ReLU activation functions, and 0.2 dropout after the second layer. The output of these two mlps were then concatenated and this vector was then passed through a mlp consisting of 4 layers with 128, 128, 64, and 1 neurons. The first 3 layers had an ReLU activation function and the 2nd layer had 0.2 dropout applied. The late fusion model first consisted of two identical mlp's for the hydrophone and microphone frequency feature vectors. These models had 5 layers with 200, 200, 200, 200, and 64 neurons, all with ReLU activation functions. A dropout layer with a rate of 0.2 is applied after the 2nd and 4th layer. The output of these mlps are concatenated and then passed through a single dense layer with one neuron. All of the models used the mean squared error loss function and the Adam optimizer. They were trained with a patience of 10 and the weights corresponding to the best validation loss were restored. These five machine learning model structures were implemented using TensorFlow [28].

Layer	Activation Function	Output Shape
Input		[(None, 2000)]
Dense	ReLU	(None, 200)
Dense	ReLU	(None, 200)
Dropout		(None, 200)
Dense	ReLU	(None, 200)
Dense	ReLU	(None, 200)
Dropout	-	(None, 200)
Dense	ReLU	(None, 64)
Dropout		(None, 64)
Dense		(None, 1)

FIGURE 4: MODEL ARCHITECTURE USED FOR BOTH THE HYDROPHONE ONLY AND MICROPHONE ONLY MODELS.

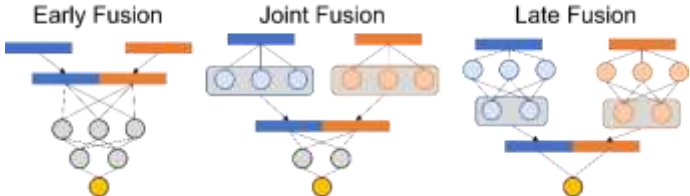


FIGURE 5: SCHEMATIC SHOWING THE GENERAL FUSION PROCESSES

Gaussian process regression (GPR), another supervised machine learning regression model architecture, was also implemented. Gaussian process regression is a probabilistic model in which a kernel is defined and used for calculating the covariance matrix used in fitting the data. Three different Gaussian models were trained; one using only the hydrophone frequency intensity data, one using only microphone frequency intensity data, and one used both data types. All three models used the same kernel: DotProduct() + WhiteKernel() + ConstantKernel().

where

$$\begin{aligned} & \textit{DotProduct:} \, k\big(x_i, x_j\big) = \sigma_0^2 + x_i \cdot x_j & ; \\ & \textit{WhiteKernel:} \, k\big(x_i, x_j\big) = \begin{cases} 1 \, \text{if} \, x_i == x_j \\ 0 & ; \end{cases} \\ & \textit{ConstantKernel:} \, k\big(x_i, x_j\big) = 1.0. \end{aligned}$$

For the combined model, the microphone and hydrophone frequency features for each corresponding heat flux were appended together. This model is referred to as the early fusion Gaussian model. These models were implemented using the Scikit-learn library [29] in python.

Five different supervised mlp models were trained. One mlp for hydrophone data only, one mlp for microphone data only and three fusion models combining both data types for predicting

3. RESULTS AND DISCUSSION

3.1 Model Performance

heat flux. For all the model types using microphone data, both the filtered and raw signals were used for training and testing. Figure 6 shows the coefficient of determination (R² score) for the models calculated from the test data. The R² score is defined as $R^2 = 1 - \frac{\sum_{i=1}^{N} (True_i - Pred_i)^2}{\sum_{i=1}^{N} (True_i - Mean)^2}$. This is a measurement of the fit of the model to the data, where an R² of 1 is the best scenario and values close to one are desired indicating the model fits the data well. From this bar plot a couple things can be seen. The model just using the hydrophone data performs better than the models just using the microphone signals. It is also observed that the mlp model with the filtered microphone data performs worst when trained and tested with raw signal data than the filtered data. However, this is not the case for the three fusion models. For the joint and late fusion types, the model using filtered microphone data performed better than the one with the raw signal. It is also seen that with the exception of the noisy early fusion model, all the fusion models preform better than the non-fused models. For the raw microphone data, the best model was found to be the late fusion model achieving a R² score of 0.982 on the test data. While the best model using the filtered microphone signal was found to be the late fusion model with a R² score of 0.985. Figure 7 shows the predicted heat flux vs the true heat flux label for all the models using the log scale on both axes. Ideally, the predicted heat flux would equal the true heat flux label so all the points would reside on the diagonal black line. These plots make sense given the R² scores. For example, the plot of predicted vs true for the microphone only model's points are spread out more than the best performing late fusion model with filter microphone data whose points more closely follow the diagonal line. Another area where the mlp models were compared was their training times. Figure 8 shows the total training times for each model. It was found that the late fusion models took the most time for training while the microphone only models and early fusion model were the fastest.

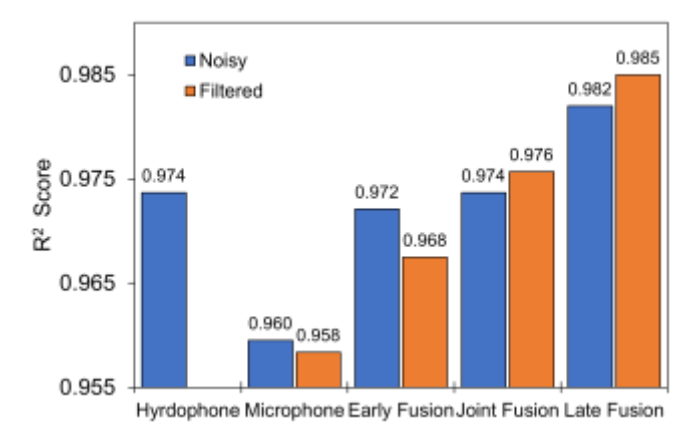


FIGURE 6: R² VALUES FOR FIVE DIFFERENT MODELS; HYDROPHONE MLP, MICROPHONE MLP, EARLY FUSION, JOINT FUSION, AND LATE FUSION WITH BOTH RAW DATA AND FILTERED DATA.

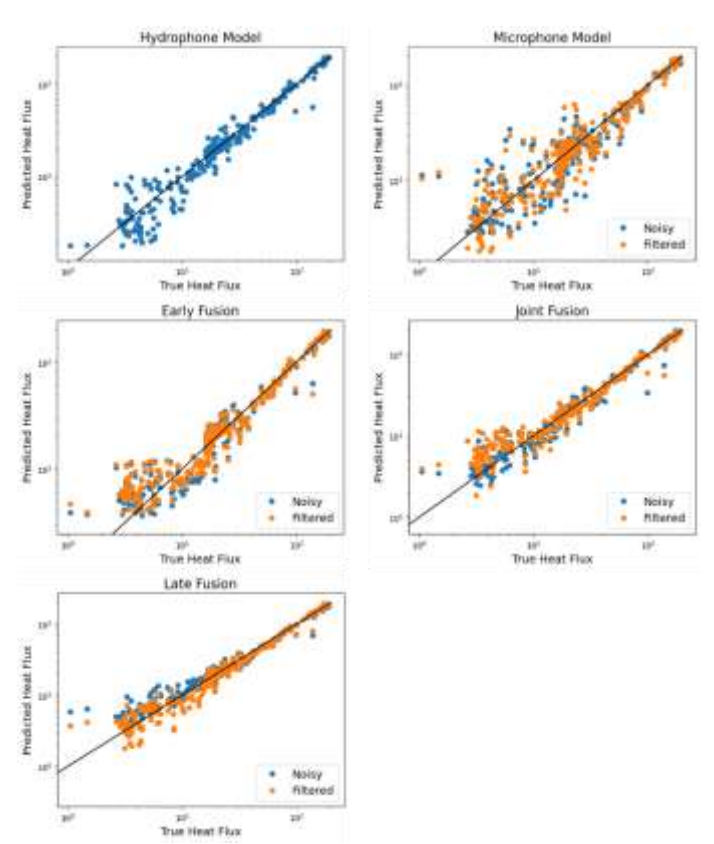


FIGURE 7: PREDICTED VS. TRUE HEAT FLUX FOR ALL MLP MODELS; HYDROPHONE DATA ONLY, MICROPHONE DATA ONLY, EARLY FUSION, JOINT FUSION, AND LATE FUSION.

Three Gaussian process regression models were also trained and tested using the same data. **Figure 9** shows the R² score for these three gpr models. As seen by this plot the noise filtering performed on the microphone data did not improve the performance for either of the models including microphone data.

The early fusion model using the noisy microphone data performed the best with an R^2 score of 0.985. This value was the highest achieved among all of the models including the mlp ones. However, when compared to the mlp models both the hydrophone data only and microphone data only gpr models had lower R^2 scores.

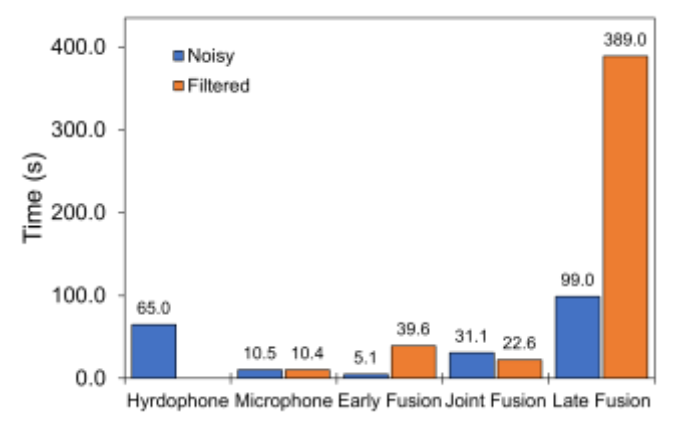


FIGURE 8: TRAINING TIMES FOR THE FIVE DIFFERENT MODELS; HYDROPHONE MLP, MICROPHONE MLP, EARLY FUSION, JOINT FUSION, AND LATE FUSION WITH BOTH RAW DATA AND FILTERED DATA.

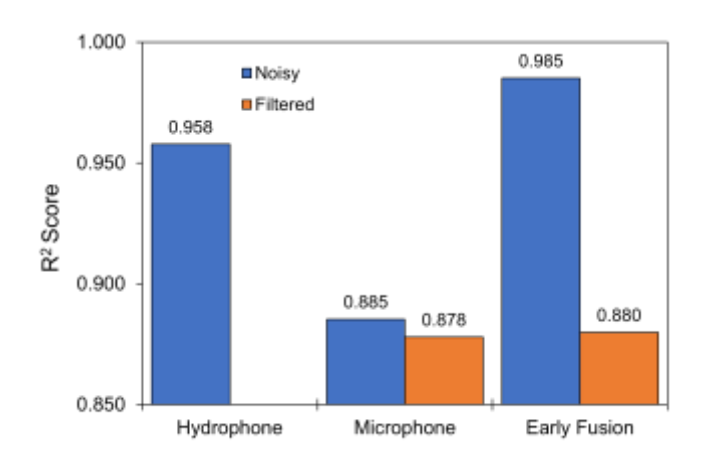


FIGURE 9: R² SCORE OF ALL GAUSSIAN PROCESS REGRESSION MODELS. SHOWS VALUES FOR HYDROPHONE DATA ONLY MODEL, MICROPHONE DATA ONLY MODEL WITH FILTERED AND UNFILTERED DATA, AND BOTH FUSION MODELS WITH FILTERED AND UNFILTERED MICROPHONE DATA.

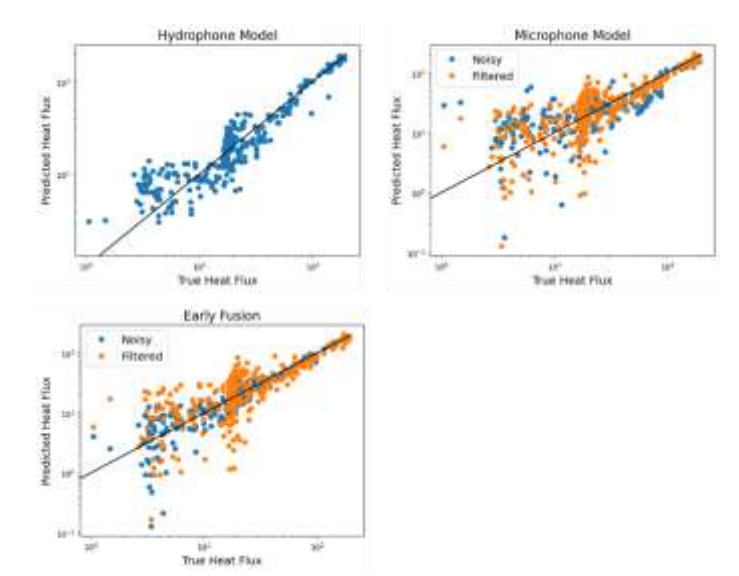


FIGURE 10: PREDICTED VS. TRUE HEAT FLUX FOR ALL GAUSSIAN MODELS; HYDROPHONE DATA ONLY, MICROPHONE DATA ONLY, EARLY FUSION MODEL.

3.1 Hydrophone and Microphone Signal Comparison

Although both acoustic sensors are used to measure the same experiment, the models all performed differently. One thing of note is that for the mlp models with hydrophone data and the hydrophone gpr model there are two predicted heat flux points that deviate more than 30 W/cm² from the true value. These two outstanding points are present in all of the mlp models with hydrophone data. To look into this more the time at which these points are taken is found. It happens that these are the first two heat flux values in the testing set that occur after the critical heat flux is reached. At this point the heat flux decreases hundreds of degrees in a matter of seconds. Figure 11 shows the true value of these two points and the predicted value from the hydrophone only and microphone only model with respect to the heat flux curve. It is seen here that both of these points reside on the sharp decline of heat flux seen once CHF is hit. One reason for this far off prediction could be the lack of training data with in this region for the models. For both values the microphone only model prediction is closer to the true value. It is also interesting to note that for the gpr models, the hydrophone only data model also has large error in the prediction of these points but when fused the Gaussian model is able to more accurately predict them. This observation seen in both model architecture types implies that for this data preparation method, the microphone data can better predicted heat flux in the transition boiling regime than the hydrophone data.

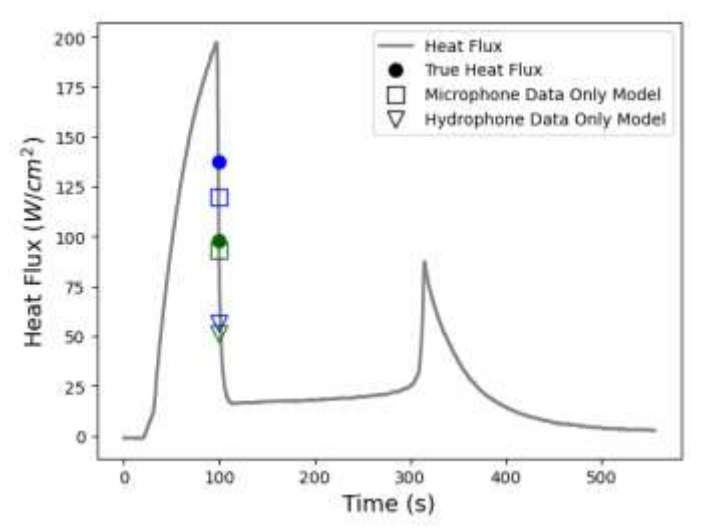


FIGURE 11: PLOT OF HEAT FLUX WITH TWO OUTSTANDING POINTS IN MODEL PREDICTION SHOWN. THESE TWO POINTS ARE MARKED ALONG WITH THE PREDICTION FROM THE HYDROPHONE DATA ONLY MLP MODEL AND THE MICROPHONE DATA ONLY MLP MODEL. THESE TWO POINTS OCCUR JUST AFTER THE MAX HEAT FLUX IS ACHIEVED.

Just looking at the results plots from the models trained with only one type of data, it can be observed that the hydrophone models perform better than the microphone models with a higher R² score than both with and without filtering. This is what was expected since the condenser microphone is subject to higher levels of noise and since the hydrophone is in such close proximity to the boiling surface. This is also seen in figure 12 of the spectrograms. Figure 12a shows the spectrogram from the hydrophone signal. From this, it can be seen that frequencies under 600 Hz vary the most throughout the transient experiment. Although this transition over time can easily be seen in the hydrophone data, it is less seen in figure 12b or 12c which are the spectrograms of the raw microphone signal and filtered microphone signal, respectively. In fact, there are several low frequencies of roughly constant high intensities throughout the entire time of the recording for the microphone data. For example, the dark red line at just under 300 Hz. This constant intensity frequency line can also be seen at the beginning and end of the hydrophone signal spectrogram but it is much less intense in comparison to the other frequencies present. These steady frequencies are less intense in the filtered microphone data spectrogram than the raw microphone data but the filtered microphone data also losses quite a bit of frequency information. The spectrograms are generated using the matplotlib library [30].

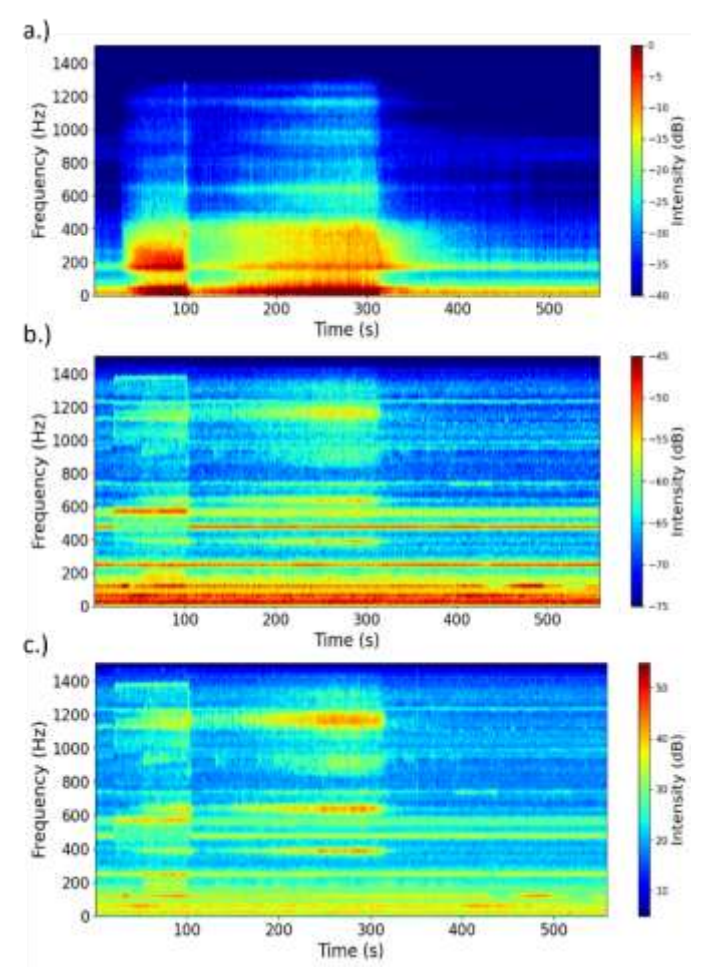


FIGURE 12: SPECTROGRAM OF THE ACOUSTIC SIGNALS FROM A.) HYDROPHONE, B.) MICROPHONE, AND C.) FILTERED MICROPHONE.

Another comparison made between the acoustic signals is the root mean squared (RMS) values. RMS is essentially a measure of loudness. The RMS value is defined as RMS =

 $\sqrt{\frac{1}{N}}\sum_{n}|x(n)|^2$. **Figure 13a** shows the heat flux vs time and the plots in **figures 13b, 13c**, and **13d** show the RMS value vs time for the hydrophone, raw microphone, and filtered microphone data. For these plots the hydrophone, microphone, and filtered microphone signals were normalized to be between -1 and 1. For the RMS values data from overlapping windows are used to generate the RMS vs time plot. From these plots it can be seen that both microphone and hydrophone signals show an increase in volume as the heat flux rises to the critical heat flux. Both signals also show a sharp decline in RMS after the critical heat flux has been reached. The RMS values are found using the librosa library [31].

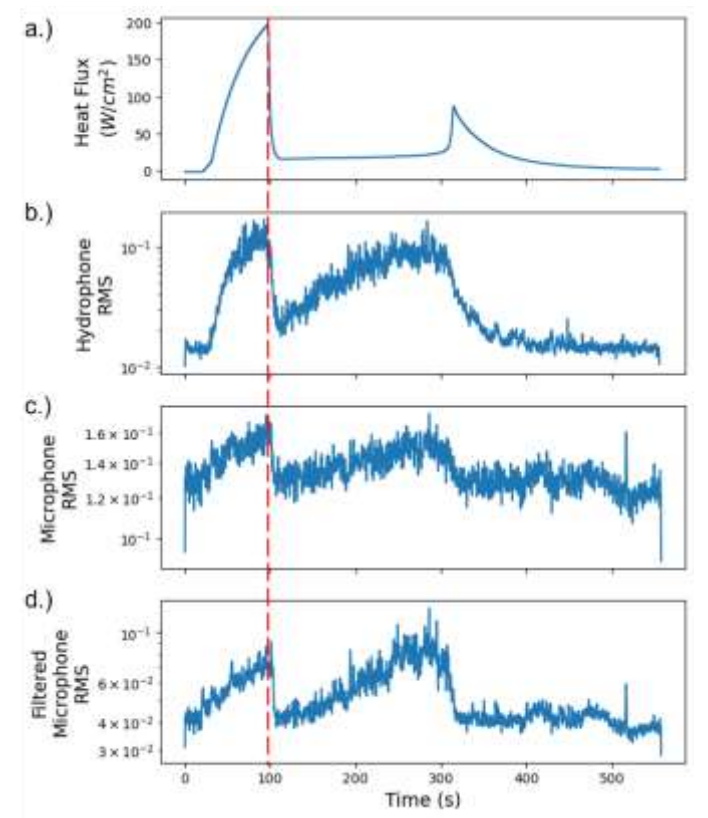


FIGURE 13: FOUR PLOTS FOR COMPARING A.) THE CALCULATED HEAT FLUX VS TIME, B.) RMS VS TIME FOR THE HYDROPHONE DATA, C.) RMS VS TIME FOR THE MICROPHONE DATA, AND D.) RMS VS TIME FOR THE FILTERED MICROPHONE DATA. THE RED DASHED LINE SHOWS THE TIME CORRESPONDING TO THE CRITICAL HEAT FLUX.

4. CONCLUSION

Acoustic signals from pool boiling can be used to approximate heat flux. Hydrophone and microphone signals contain frequency information that correlates to the heat flux of the system. Hydrophone data achieves the best accuracy when compared to the condenser microphone due to its proximity to the boiling surface and smaller noise levels. However, even with the high levels of noise present in the condenser microphone signal, the regression models still performed well with some R² scores greater than 0.95. It was also seen that the noise removal process used did not improve the accuracy of the individual models. It was also found that fusing the two signal types together shows promise in achieving even higher prediction accuracy. It is important to note that although the models performed well with the experimental test data, they are expected to have less accurate results for additional experiments with different boiling liquids, heating surface, or even background noise. Future studies will involve incorporating more data from separate experiments to attempt and create a more generalizable model.

ACKNOWLEDGEMENTS

This study was supported by the National Science Foundation under Grant No. TI-2212002 and the University of Arkansas through the Chancellor's Commercialization Fund and GAP Fund. This work used Bridges2 GPU at Pittsburgh Supercomputing Center through allocation MCH200010 from the Advanced Cyberinfrastructure Coordination Ecosystem: Services & Support (ACCESS) program, which is supported by National Science Foundation grants #2138259, #2138286, #2138307, #2137603, and #2138296. J.M. and E.W. appreciate support from the University of Arkansas Honors College Research Grant.

REFERENCES

- [1] Q. Zhang *et al.*, "A survey on data center cooling systems: Technology, power consumption modeling and control strategy optimization," *Journal of Systems Architecture*, vol. 119, p. 102253, Oct. 2021, doi: 10.1016/J.SYSARC.2021.102253.
- [2] C. Roe *et al.*, "Immersion cooling for lithium-ion batteries A review," *J Power Sources*, vol. 525, p. 231094, Mar. 2022, doi: 10.1016/J.JPOWSOUR.2022.231094.
- [3] H. Hu, J. A. Weibel, and S. V. Garimella, "A coupled wicking and evaporation model for prediction of pool boiling critical heat flux on structured surfaces," *Int J Heat Mass Transf*, vol. 136, pp. 373–382, 2019, doi: 10.1016/j.ijheatmasstransfer.2019.03.005.
- [4] J. P. McHale and S. v. Garimella, "Nucleate boiling from smooth and rough surfaces Part 1: Fabrication and characterization of an optically transparent heater-sensor substrate with controlled surface roughness," *Exp Therm Fluid Sci*, vol. 44, pp. 456–467, Jan. 2013, doi: 10.1016/j.expthermflusci.2012.08.006.
- [5] M. M. Rahman, E. Ölçeroglu, and M. McCarthy, "Role of wickability on the critical heat flux of structured superhydrophilic surfaces," *Langmuir*, vol. 30, no. 37, pp. 11225–11234, Sep. 2014, doi: 10.1021/la5030923.
- [6] M. Bongarala, H. Hu, J. A. Weibel, and S. V Garimella, "Microlayer evaporation governs heat transfer enhancement during pool boiling from microstructured surfaces," *Appl Phys Lett*, vol. 221602, no. May, 2022, doi: 10.1063/5.0090156.
- [7] L. A. Konopko, A. A. Nikolaeva, T. E. Huber, and A. K. Kobylianskaya, "Miniaturized Heat-Flux Sensor Based on a Glass-Insulated Bi–Sn Microwire," *Semiconductors*, vol. 53, no. 5, pp. 662–666, May 2019, doi: 10.1134/S1063782619050117.
- [8] C. Dunlap, H. Pandey, and H. Hu, "Supervised and Unsupervised Learning Models for Detection of Critical Heat Flux during Pool Boiling," in *Proceedings of the* ASME 2022 Heat Transfer Summer Conference, Philadelphia, PA, 2022.
- [9] A. Rokoni, L. Zhang, T. Soori, H. Hu, T. Wu, and Y. Sun, "Learning new physical descriptors from reduced-order analysis of bubble dynamics in boiling heat transfer," *Int*

- *J Heat Mass Transf*, vol. 186, p. 122501, 2022, doi: 10.1016/j.ijheatmasstransfer.2021.122501.
- [10] S. M. Rassoulinejad-Mousavi *et al.*, "Deep learning strategies for critical heat flux detection in pool boiling," *Appl Therm Eng*, vol. 190, p. 116940, 2021, doi: 10.1016/j.applthermaleng.2021.116849.
- [11] J. P. McHale and S. v. Garimella, "Nucleate boiling from smooth and rough surfaces Part 2: Analysis of surface roughness effects on nucleate boiling," *Exp Therm Fluid Sci*, vol. 44, pp. 439–455, Jan. 2013, doi: 10.1016/j.expthermflusci.2012.08.005.
- [12] Y. Suh, R. Bostanabad, and Y. Won, "Deep learning predicts boiling heat transfer," *Sci Rep*, vol. 11, no. 1, pp. 1–11, 2021, doi: 10.1038/s41598-021-85150-4.
- [13] G. M. Hobold and A. K. da Silva, "Visualization-based nucleate boiling heat flux quantification using machine learning," *Int J Heat Mass Transf*, vol. 134, pp. 511–520, May 2019, doi: 10.1016/J.IJHEATMASSTRANSFER.2018.12.170.
- [14] H. Hu, H. Pandey, and C. Dunlap, "Detecting or Predicting System Faults in Cooling Systems in a Non-Intrusive Manner Using Deep Learning," Dec 9, 2022, US Patent Application No. 18/078,774.
- [15] T. Alhashan, A. Addali, J. Amaral Teixeira, and S. Elhashan, "Identifying bubble occurrence during pool boiling employing acoustic emission technique," *Applied Acoustics*, vol. 132, pp. 191–201, Mar. 2018, doi: 10.1016/j.apacoust.2017.11.006.
- [16] S. H. Baek, K. Wu, H. S. Shim, D. H. Lee, J. G. Kim, and D. H. Hur, "Acoustic emission monitoring of water boiling on fuel cladding surface at 1 bar and 130 bar," *Measurement (Lond)*, vol. 109, pp. 18–26, Oct. 2017, doi: 10.1016/j.measurement.2017.05.042.
- [17] K. Nishant Ranjan Sinha, D. Ranjan, N. Kumar, M. Qaisar Raza, and R. Raj, "Simultaneous audio-visual-thermal characterization of transition boiling regime," *Exp Therm Fluid Sci*, vol. 118, Oct. 2020, doi: 10.1016/j.expthermflusci.2020.110162.
- [18] F. König, C. Sous, A. Ouald Chaib, and G. Jacobs, "Machine learning based anomaly detection and classification of acoustic emission events for wear monitoring in sliding bearing systems," *Tribol Int*, vol. 155, Mar. 2021, doi: 10.1016/j.triboint.2020.106811.
- [19] M. Comunità, D. Stowell, and J. D. Reiss, "Guitar Effects Recognition and Parameter Estimation with Convolutional Neural Networks," Dec. 2020, doi: 10.17743/jaes.2021.0019.
- [20] G. Forte, F. Alberini, M. Simmons, and H. E. Stitt, "Use of acoustic emission in combination with machine learning: monitoring of gas—liquid mixing in stirred tanks," *J Intell Manuf*, vol. 32, no. 2, pp. 633–647, Feb. 2021, doi: 10.1007/s10845-020-01611-z.

- [21] K. N. R. Sinha, V. Kumar, N. Kumar, A. Thakur, and R. Raj, "Deep learning the sound of boiling for advance prediction of boiling crisis," *Cell Rep Phys Sci*, vol. 2, no. 3, p. 100382, 2021, doi: 10.1016/j.xcrp.2021.100382.
- [22] Y. Ueki and K. Ara, "Proof of concept of acoustic detection of boiling inception and state transition using deep neural network," *International Communications in Heat and Mass Transfer*, vol. 129, Dec. 2021, doi: 10.1016/j.icheatmasstransfer.2021.105675.
- [23] A. Negi, "Characterization of Boiling Sound at Conditions Approaching Characterization of Boiling Sound at Conditions Approaching Critical Heat Flux Critical Heat Flux," 2019. [Online]. Available: https://scholarworks.rit.edu/theses
- [24] H. Pandey, H. Mehrabi, A. Williams, C. Mira-Hernández, R. H. Coridan, and H. Hu, "Electrochemical Control of Copper Foam Synthesis for Critical Heat Flux Enhancement During Boiling," Available at SSRN: https://ssrn.com/abstract=4382894 or http://dx.doi.org/10.2139/ssrn.4382894.
- [25] H. Pandey, C. Dunlap, A. Williams, J. Marsh, and H. Hu, "Multimodal characterization of steady-state and transient boiling heat transfer," in *Proceedings of the ASME 2023 Heat Transfer Summer Conference*, 2023, pp. HT2023-106015.
- [26] H. Pandey, W. Waldo, and H. Hu, "Non-Intrusive Cooling System Fault Detection and Diagnostics Using Acoustic Emission," in *Proceedings of the ASME 2022 Heat Transfer Summer Conference*, Philadelphia, PA, 2022, pp. HT2022-85429.
- [27] C. R. Harris *et al.*, "Array programming with NumPy," *Nature*, vol. 585, no. 7825. Nature Research, pp. 357–362, Sep. 17, 2020. doi: 10.1038/s41586-020-2649-2.
- [28] M. Abadi *et al.*, "TensorFlow: A system for large-scale machine learning," May 2016, [Online]. Available: http://arxiv.org/abs/1605.08695
- [29] F. Pedregosa FABIANPEDREGOSA *et al.*, "Scikit-learn: Machine Learning in Python Gaël Varoquaux Bertrand Thirion Vincent Dubourg Alexandre Passos PEDREGOSA, VAROQUAUX, GRAMFORT ET AL. Matthieu Perrot," 2011. [Online]. Available: http://scikit-learn.sourceforge.net.
- [30] J. D. Hunter, "Matplotlib: A 2D graphics environment," *Comput Sci Eng*, vol. 9, no. 3, pp. 90–95, 2007, doi: 10.1109/MCSE.2007.55.
- [31] B. McFee *et al.*, "librosa: Audio and Music Signal Analysis in Python," in *Proceedings of the 14th Python in Science Conference*, SciPy, 2015, pp. 18–24. doi: 10.25080/majora-7b98e3ed-003.